The Effects of Land-Use Alteration on the Sea Breeze and Daytime Heat Island in the Tokyo Metropolitan Area

By Hiroyuki Kusaka

Environmental Science Department, Central Research Institute of Electric Power Industry, Japan

Fujio Kimura

Institute of Geoscience, University of Tsukuba, Japan

Hiromaru Hirakuchi and Masafumi Mizutori

Environmental Science Department, Central Research Institute of Electric Power Industry, Japan

(Manuscript received 29 October 1999, in revised form 4 April 2000)

Abstract

The changes of a sea breeze and a daytime heat island due to land-use alteration during an 85 year period (1900–1985) have been numerically simulated. The domain of interest is the Kanto Plain (15000 km^2), including the Tokyo metropolitan area. This urban area is located in the southern part of the plain and consists of many cities in Tokyo and its suburbs. The horizontal scale of the area is about 40 km and has increased by a factor of four during the 85 year period. The simulations were conducted under a summer synoptic condition with weak gradient wind and almost clear sky. The model is based on the three-dimensional anelastic equations, taking into account the hydrostatic assumption. First, it was confirmed that the simulated wind field and temperature distribution with using the land-use data for 1985, agreed with observed data. The simulations were then conducted using the land-use data for 1950 and 1900. From comparison among the three simulations, the following two major conclusions were obtained: (1) Land-use alteration modified the wind system over the Kanto Plain. In particular, the simulated sea breeze front in 1985 was more clearly defined around the northern end of the Tokyo metropolitan area. The time required for the sea breezes to reach inland areas increased by two hours. (2) The warming due to land-use alteration is found over the Tokyo metropolitan area and the northwestern part of the Kanto Plain. In particular, the area of the most prominent warming is found in the northern end of the Tokyo metropolitan area. Intensity of daytime heat island in the area were estimated as 3–4°C and 2–3°C during the 85 year period, and latest 35 years respectively. The above warming is confirmed to result from the enhanced sensible heat flux and the change of interaction between the boundary layer heating and sea breeze front.

1. Introduction

Land-use alteration modifies the local climate. In particular, it is well known that temperature in an urban area tends to increase over a long period of time, accompanied by wind convergence in the area. The Tokyo metropolitan area is located in the southern part of the Kanto Plain and consists of many cities in Tokyo and its suburbs. This area had a horizontal scale of about 40 km in 1985, 25 km in 1950, and 10 km in 1900. The population in this area is about twenty million, a tenfold increase since 1900. From these facts, it can be seen that the Tokyo metropolitan area has rapidly developed into one of the largest urban areas in the world during the 85 year period. Fujibe (1994) found the widespread warming over the Kanto Plain in the daytime of the warm season (April–September). Figure 1 shows the change of the daily maximum temperature in summer over the year 1946–1976. From this figure, it is found that the daily maximum temperature averaged for July–August in the central-northwestern

Corresponding author: Hiroyuki Kusaka, Abiko Research Laboratory, Central Research Institute of Electric Power Industry, 1646 Abiko, Abiko-shi, Chiba-ken, 270-1194, Japan. E-mail: h-kusaka@criepi.denken.or.jp
©2000, Meteorological Society of Japan

part of the Kanto Plain, had increased by 1–1.5°C over the 30 years. Fujibe and Asai (1980) analyzed observed wind data under near calm conditions and discovered a local wind convergence over the Tokyo metropolitan area. It was also reported that the speed of the climatological mean convergent wind toward the city was about 0.2 m s^{-1} which was an anomaly from values horizontally averaged in the area. Yoshikado and Kondo (1989) observed the features that the sea breeze front was formed over the Tokyo metropolitan area, and its advance was much slower over the area by the effect of the daytime heat island.

The above observational and analytical studies provide us with important and basic generalization as to the local climate change with urbanization.

On the other hand, it is possible to estimate the effect of land-use on local climate by use of a three-dimensional meso-scale model (Bornstein 1986). Realistic three-dimensional simulations of urban effects were carried out by Hjelmfelt (1982), Seaman et al. (1989), Kimura and Takahashi (1991), Ichinose et al. (1999), and Taha et al. (1999). Kimura and Takahashi (1991) carried out numerical simulations of the Tokyo metropolitan area under typical summer synoptic conditions, with and without land-use data and anthropogenic heat. From a comparison of these simulations, it was found that the intensity of the Tokyo daytime heat island was about 1°C; the daytime heat island mainly formed by the decrease of latent heat release from the surface. Ichinose et al. (1999) also reached a similar conclusion using maps of the land-use and anthropogenic heat with higher resolution.

Most of the sensitivity experiments have been carried out as the theoretical studies by comparison of two runs using the realistic current land-use data, and those without urban area in order to estimate urban effects. One of the present interests is to examine the historical changes of a daytime heat island and a sea breeze associated with the development of the urban area by using realistic land-use data of the past. It is also of interest to compare the simulated wind field and temperature distribution with observed data, although the horizontal resolution of the model is not high enough to simulate values depending on the local effects of buildings, terrain, and land-use on the observation site. The main purpose of this study is to numerically estimate the historical changes of a daytime heat island, and a sea breeze in the Tokyo metropolitan area, by using realistic land-use data for the period around 1985, 1950, and 1900. Furthermore, the paper presents the relationship between the sea breeze front modified by the land-use alteration and the daytime heat island.

Abrief description of the numerical model is given in Section 2, with a description of the land-use data presented. The results of three numerical simulations are discussed in Section 3, and remarks and conclusions follow in Section 4.

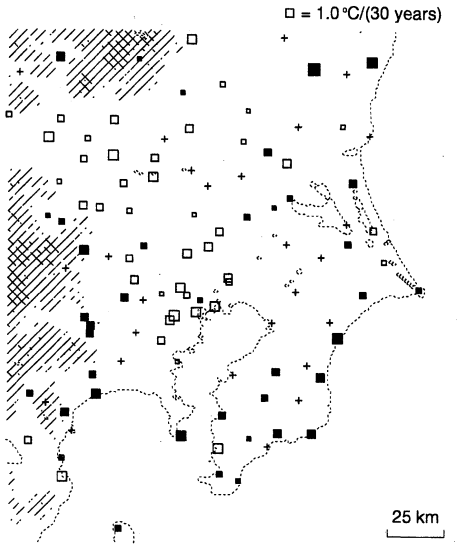

Fig. 1. Distribution of long-term change rate of daily maximum temperature averaged for July–August during the period 1946–1976. The open and closed squares indicate positive and negative trends, respectively, with their areas proportional to the absolute values of change rate. Crosses indicate change rates from −0.2°C/ (30 years) to +0.2°C/ (30 years) (by courtesy of F. Fujibe).

2. Numerical model and land-use data

2.1 Numerical model

The numerical model used in the present study is a modified version of the Local Circulation Model (LCM) used in Kimura and Arakawa (1983), and Kimura and Takahashi (1991). The basic features of the LCM adapted to the present study are summarized in Table 1. The following is a brief description of the model. Further discussion of surface heat, moisture and momentum fluxes and solar radiation can be found in Kimura and Arawaka (1983), and Kimura and Takahashi (1991). The model equations are the anelastic hydrostatic equations (Ogura and Phillips 1962).

The equations of motion are written as

$$\frac{\partial u}{\partial t} + u\frac{\partial u}{\partial x} + v\frac{\partial u}{\partial y} + w\frac{\partial u}{\partial z} = fv - \Theta\frac{\partial \pi'}{\partial x} + \frac{\partial}{\partial x}\left(K_H\frac{\partial u}{\partial x}\right) + \frac{\partial}{\partial y}\left(K_H\frac{\partial u}{\partial y}\right) + \frac{\partial}{\partial z}\left(K_m\frac{\partial u}{\partial z}\right), \quad (1)$$

and

$$\frac{\partial v}{\partial t} + u\frac{\partial v}{\partial x} + v\frac{\partial v}{\partial y} + w\frac{\partial v}{\partial z}$$

Table 1. Basic features of the model.

Basic equations	Anelastic hydrostatic equations (Ogura and Phillips, 1962)
Planetary boundary layer	Turbulent closure model at level 2 (Mellor and Yamada, 1974)
Constant flux layer	Monin-Obukhov similarity theory
Surface temperature	Force-Restore method (Bhumralkar, 1975)
Short-wave radiation	(Kimura and Arakawa, 1983)
Long-wave radiation	Empirical form (Kondo et al., 1991)
Top boundary condition	Wave radiation condition (Klemp and Durran, 1983)
Lateral boundary condition	Wave radiation condition (Orlanski, 1976)
Vertical coordinate	Terrain-following system, where $z_* = z_T \times (z - z_G)/(z_T - z_G)$, z_G is the ground surface, z_T the top level (27 layers).
Domain size and grid	242 × 242 points, with a 2 km increment

$$= -fu - \Theta\frac{\partial \pi'}{\partial y} + \frac{\partial}{\partial x}\left(K_H\frac{\partial v}{\partial x}\right) + \frac{\partial}{\partial y}\left(K_H\frac{\partial v}{\partial y}\right) + \frac{\partial}{\partial z}\left(K_m\frac{\partial v}{\partial z}\right). \quad (2)$$

The thermodynamic equation is expressed as

$$\frac{\partial \theta'}{\partial t} + u\frac{\partial \theta'}{\partial x} + v\frac{\partial \theta'}{\partial y} + w\frac{\partial \theta'}{\partial z} = \frac{\partial}{\partial x}\left(K_H\frac{\partial \theta'}{\partial x}\right) + \frac{\partial}{\partial y}\left(K_H\frac{\partial \theta'}{\partial y}\right) + \frac{\partial}{\partial z}\left(K_h\frac{\partial \theta'}{\partial z}\right), \quad (3)$$

the equation for specific humidity as

$$\frac{\partial q}{\partial t} + u\frac{\partial q}{\partial x} + v\frac{\partial q}{\partial y} + w\frac{\partial q}{\partial z} = \frac{\partial}{\partial x}\left(K_H\frac{\partial q}{\partial x}\right) + \frac{\partial}{\partial y}\left(K_H\frac{\partial q}{\partial y}\right) + \frac{\partial}{\partial z}\left(K_h\frac{\partial q}{\partial z}\right), \quad (4)$$

the continuity equation as

$$\frac{\partial \rho_0 u}{\partial x} + \frac{\partial \rho_0 v}{\partial y} + \frac{\partial \rho_0 w}{\partial z} = 0 \quad (5)$$

and the hydrostatic equation as

$$\frac{\partial \pi'}{\partial z} = g\frac{\theta'}{\Theta^2} \quad (6)$$

The symbols have each conventional meaning (cf., Appendix). The Exner's function is defined as

$$\pi = c_p\left(\frac{p}{p_{00}}\right)^{\mathrm{R}_d/\mathrm{c}_p}. \quad (7)$$

The vertical exchange coefficients in (1)–(4) are calculated in the turbulence closure model (at level 2) developed by Mellor and Yamada (1974). Vertical coordinate is transformed from z to z^*, and written in a terrain-following coordinate system in order to consider the terrain effect in the model. The vertical coordinate z^* is defined as

$$z^* = \frac{z_T(z - z_G)}{(z_T - z_G)}. \quad (8)$$

The vertical grid interval is variable, with 27 vertical levels located at the following heights: 10, 32, 58, 89, 125, 169, 222, 283, 357, 445, 549, 673, 820, 995, 1203, 1436, 1676, 1916, 2179, 2492, 2863, 3305, 3830, 4455, 5198, 6022, and 6802 m in z^* coordinates.

The top boundary is controlled by the wave radiation condition discussed in Klemp and Durran (1983), in order to avoid the reflection of gravity waves generated in lower layers. For the lateral boundaries, the wave radiation condition given by Orlanski (1976) is applied.

Below the lowest level ($z^* = 10$ m) at the surface, a constant flux layer is assumed. The surface temperature is calculated by the force-restore method (Bhumralkar 1975; Deardorff 1978).

The net short wave radiation is calculated according to Kimura and Arakawa (1983).

The net long wave radiation is given by the empirical form (Kondo et al. 1991), estimated from Yamamoto's radiation chart (Yamamoto 1952), and a lot of data on clear sky days during summer (1979–1986 year).

The momentum flux τ, sensible heat flux H and latent heat flux lE are calculated from the following equations,

$$\tau = \rho_0 u_*^2, \quad (9)$$

$$H = -\rho_0 c_p u_* \theta_*, \quad (10)$$

and

$$lE = -\rho_0 l u_* q_*. \quad (11)$$

These variables are calculated by the Monin-Obukhov similarity theory in the constant flux layer, according to Kimura and Arakawa (1983). The iterated method is applied to obtain a solution.

2.2 Domain of calculation and land-use data

The Kanto Plain is the largest plain (15000 km^2) in Japan. The southern part of this plain includes

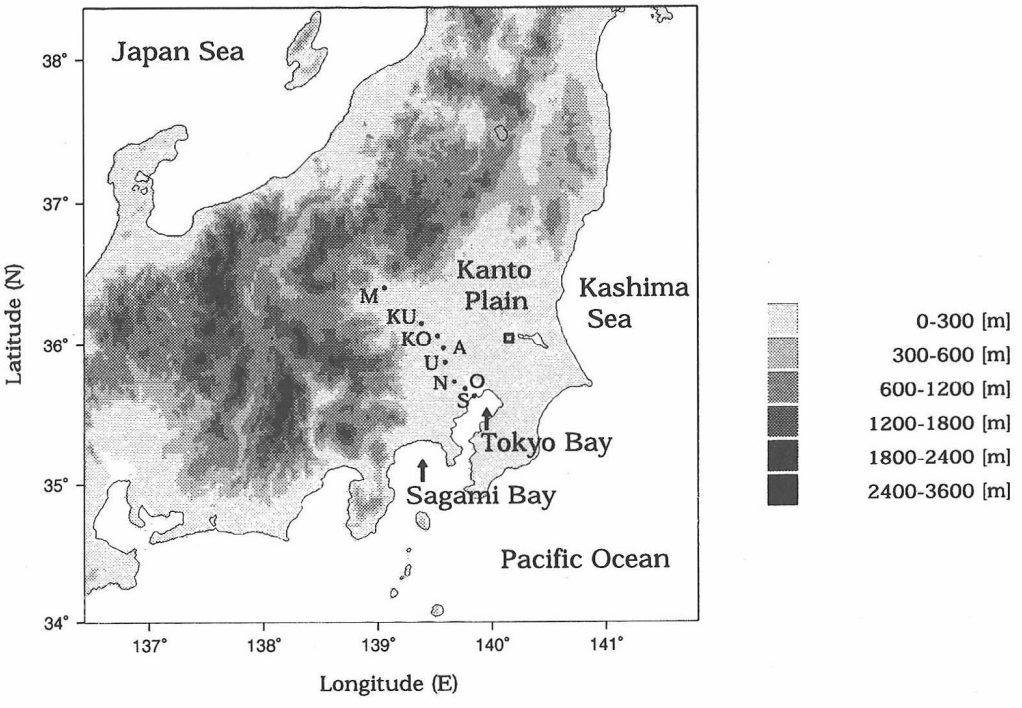

Fig. 2. Topography of the domain used in all simulation cases and site locations of the analyzed points: Shinkiba (S), Otemachi (O), Nerima (N), Urawa (U), Ageo (A), Kounosu (KO), Kumagaya (KU), and Maebashi (M). The open square indicates Tateno station.

the Tokyo metropolitan area within a radius of 20 km, which consists of many cities. The plain is surrounded by mountains having heights of greater than 2000 m to the north and west, while the Pacific Ocean borders the south and east (Fig. 2). It is well known that the usual sea breeze and so-called 'extended sea breeze', having a larger scale than the usual sea breeze, are often found over the Kanto Plain on typical summer days (Fujibe and Asai 1979; Kondo and Yoshikado 1988; Kondo 1990). The extended sea breeze is the local wind which is generated through the non-linear combination between the sea breeze and valley wind, strongly influenced by the mountains (Kondo 1990). Considering these effects, the domain for the model calculation is selected as shown in Fig. 2. The horizontal grid interval of the model is 2 km.

The present land-use types are obtained from the data set edited by Himiyama (1998). The mesh size of the data is roughly 2 km by 2 km, and the data set contains land-use data for the periods, around the year 1985, 1950 and 1900. The major information source of this data set has been 1:50000 topographic maps produced during three periods by the predecessors of the current Land Agency. First, each of some 4000 maps covering the whole country in the three periods was colored according to the land-use, or land-cover type identified from the symbols and other clues on the maps. Then land use information was read and recorded in Laster form for each of the grid squares drawn on the maps. The land-use maps of the Kanto Plain around the year 1985, 1950, and 1900 are shown in Figs. 3a, 3b, and 3c, respectively. Table 2 shows the land-use classification used in this study and that defined by Himiyama (1998). The ratio of each category to the area shown in Fig. 3 for each period is listed in Table 3. The urban area in 1985 was about seven times greater than that in 1900, and about twice that in 1950. Paddy fields have increased, while surfaces of grassland, forest, and water surface have decreased during the 85 year period. The values of the radiation parameters, i.e., the surface albedo α and the slab emissivity ε of the five categories are shown as in Table 4. The values of the surface parameters, i.e., the roughness parameter z_0, the sub-layer Stanton number St^{-1}, moisture availability β, heat capacity $c_s\ \rho_s$ and heat conductivity λ_s for each of the five categories, are assumed in Table 5. The parameters were quoted from the values observed in the central Japan (i.e., Kondo and Yamazawa 1986; Kondo and Watanabe 1992; Nakagawa and Ooi 1992), and from Garratt (1978), and Anthes et al. (1987). It was confirmed that the results obtained by the run with the above mentioned parameters were similar to those obtained by the run with only the parameters recommended by Anthes et al. (1987) as far as this simulation was concerned. It should be noted that anthropogenic heat is not taken into consideration in order to focus attention on the effects of land-use alteration

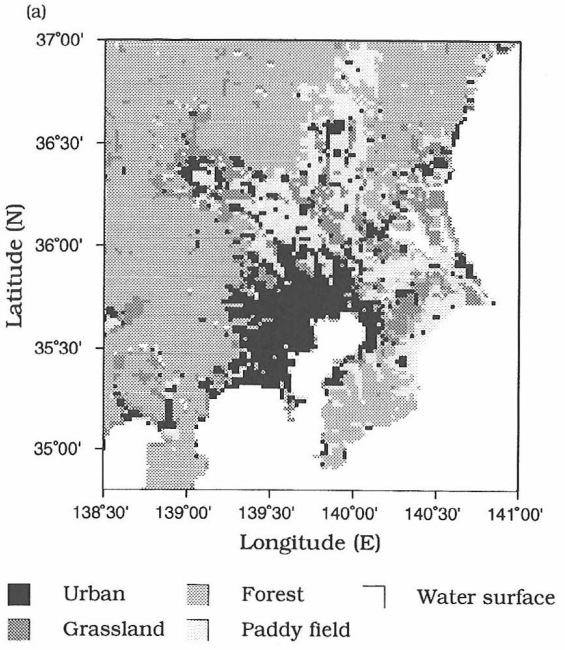

Fig. 3a. Land-use categories over the Kanto Plain. The degrees of shading indicate urban, grassland, paddy field, forest, and water surface according to the figure legend. Land-use is given for 1985.

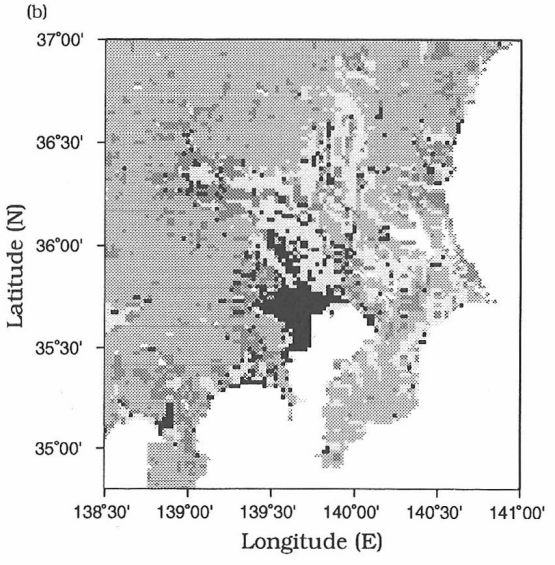

Fig. 3b. Same as Fig. 3a, but for 1950.

on the changes of a sea breeze and a daytime heat island.

2.3 Initial condition

Simulations of local wind system and temperature distribution for 1985, 1950, and 1900 are referred to as Case 1, Case 2, and Case 3. The numerical integration for all simulations is started at 0300 Local Solar Time (LST) under the following weather conditions: (1) weak gradient wind (Kondo and Yoshikado 1988), and (2) an almost clear sky. It is considered that these are necessary conditions for the appearance of a clear urban heat island. To initialize the atmosphere, the data on seven clear calm summer days, which satisfy the condition of Table 6, are used. Surface air temperature data from 55 AMeDAS (Automated Meteorological Data Acquisition System) stations of the Japan Meteorological Agency over the Kanto Plain and sonde data at Tateno station (Fig. 2) on the seven clear calm summer days taken from the years 1984 to 1985 are used for all simulations. Observed data used in later sections are also averaged values over the seven summer days. Potential temperature profiles above 1000 m are based on the least squares method using sonde data at 0900 Japan Standard Time (JST) (0000 Z) and 2100 JST (1200 Z). In a similar way, potential temperature profiles below 1000 m are estimated, using 55 mean AMeDAS data at 0300 JST. This lapse rate for the potential temperature is in rough agreement with typical values on clear days during midsummer (i.e., Gamo 1985; Yoshikado and Kondo 1989). The initial vertical profile of water vapor mixing ratio is also estimated by the least squares method using sonde data at 0900 JST (0000 Z) and 2100 JST (1200 Z). Initially, a wind speed of 0 m s^{-1} is assumed at all levels. The model atmosphere is assumed to be horizontally homogeneous at initialization. The initial conditions are summarized in Table 7.

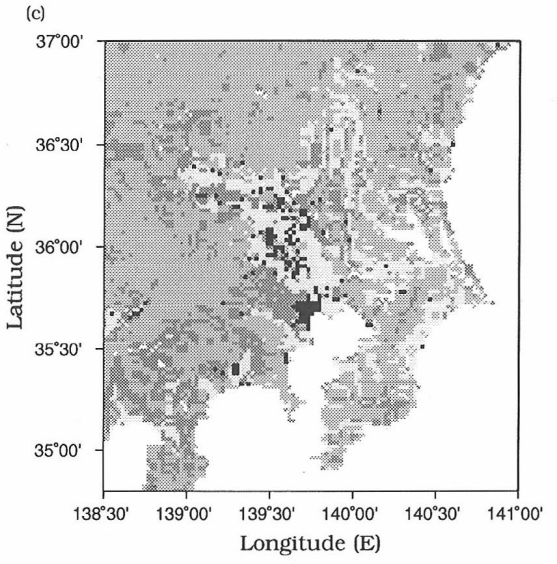

Fig. 3c. Same as Fig. 3a, but for 1900.

Table 2. Land-use classification used in this study and the original defined by Himiyama (1998).

The present study	Himiyama (1998)
Urban	Urban (Settlement, Road, Railway)
Grassland	Agricultural (Grassland, Mulberry, Tea garden, Orchard, Tree crops) and Other (Rough land, Marshy land, Golf course)
Forest	Forest (Broad-leaved forest, coniferous forest, Mixed forest, Bamboo forest)
Paddy fields	Agricultural (Paddy field)
Water surface	Other (Water)

Table 3. Land-use alteration during the 85 year period. The upper values indicate the percentage of the five categories for the three period in the area shown in Fig. 3. The lower values indicate the change in the five categories from 1900 to 1950, and to 1985.

	1900 [%]	1950 [%]	1985 [%]
Urban	1.0	3.2	7.4
	100.0	320.0	740.0
Glassland	11.6	8.6	6.1
	100.0	74.1	52.5
Forest	51.2	51.6	49.6
	100.0	100.0	96.9
Paddy fields	12.1	12.7	13.7
	100.0	105.0	113.2
Water surface	24.1	23.9	23.2
	100.0	99.2	96.3

Table 4. The five categories of classification with the assigned values of the radiation parameters.

Category	Albedo (α)	Slab emissivity (ε)
Urban	0.18	0.88
Grassland	0.19	0.92
Forest	0.15	0.93
Paddy filed	0.20	0.92
Water surface	0.08	0.98

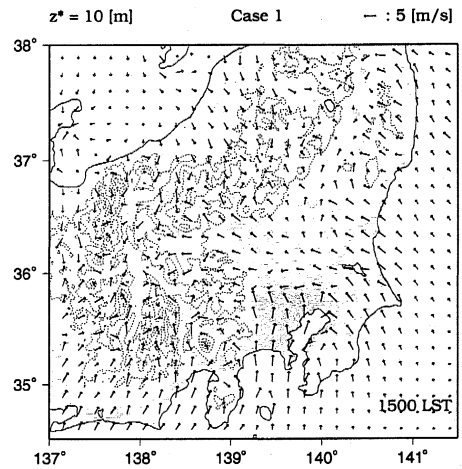

Fig. 4. Simulated wind at the $z^* = 10$ m level for 1500 LST, for Case 1. The broken lines indicate topography contour line, and the contour interval is 600 m. The shaded areas indicate the urban area.

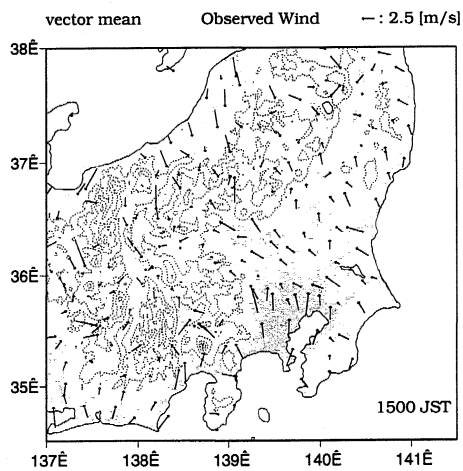

Fig. 5. Observed surface wind for 1500 JST, shown as an ensemble average of typical summer days taken from the years 1984 to 1985. The broken lines indicate topography contour line, and the contour interval is 600 m. The shaded areas indicate the urban area.

3. Results

3.1 Simulation of undisturbed summer day for 1985

The simulated surface winds (at $z^* = 10$ m) at 1500 LST for Case 1 are shown in Fig. 4, while observed surface winds from the AMeDAS are shown in Fig. 5. Here, the observed data are averaged values over the seven summer days mentioned above. It can be concluded that the simulated wind field for the summer days agrees well with the observed wind field from comparison of the two figures. The similar points are as follows.

Sea breezes originating from the Pacific Ocean, the Kashima Sea, and the Japan Sea appear in the coastal areas. Southerly winds dominate over the southern part of the Kanto Plain. The northern part of the Kanto Plain is dominated by easterly or southeasterly winds.

Figure 6 shows a scatter diagram of the simulated temperatures (at $z = 1.5$ m) at 1500 LST for Case 1 versus observed temperatures (at $z = 1.5$ m) over the

Table 5. The five categories of classification with the assigned values of the surface parameters.

Category	Roughness parameter (z_0) [m]	Stanton number (S_t^{-1})	Moisture availablility (β)	Heat capacity ($c_s\rho_s$) [cal °C^{-1} cm^{-3}]	Heat conductivity (λ_s) [cal cm^{-1} s^{-1}°C^{-1}]
Urban	0.5	6	0.05	0.49	0.0034
Grassland	0.12	6	0.15	0.49	0.0026
Forest	0.5	6	0.3	0.49	0.0026
Paddy field	0.075	6	0.6	0.49	0.0026
Water surface	0.000015	0	1	1	10

Table 6. Criteria for undisturbed summer synoptic conditions defined in this study.

Synoptic weather chart	under anticyclone conditions,
	no disturbance within 500 km of the center of the Kanto Plain
General wind speed	0–4 m s^{-1}
Duration of sunshine	7 hours over 50 % of the stations in the Kanto Plain
Precipitation	0–1 mm day^{-1} at Otemachi,
	0–1 mm day^{-1} over 70 % of the stations in the Kanto Plain
	0–5 mm hour^{-1} over 70 % of the stations in each prefecture

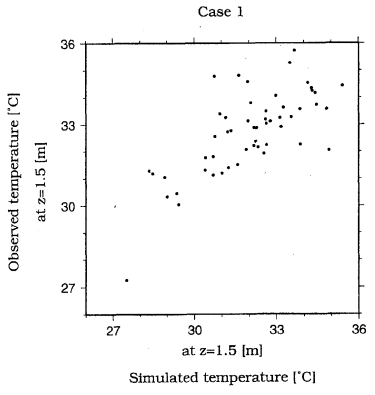

Fig. 6. Scatter diagram of the observed temperature (z = 1.5 m) at 1500 JST vs simulated temperatures (z = 1.5 m) at 1500 LST over the Kanto Plain.

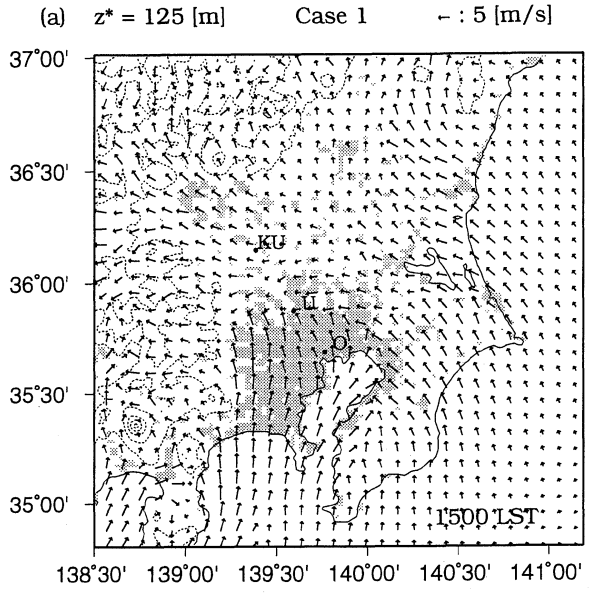

Fig. 7a. Wind velocity at the z^* = 125 m level at 1500 LST, calculated for Case 1. The broken lines indicate topography contour line, and the contour interval is 600 m. The shaded areas indicate the urban area.

Kanto Plain at 1500 JST. The simulated temperatures are interpolated vertically by Monin-Obukhov similarity theory, using lowest level temperature, the ground surface temperature, friction potential temperature, friction velocity and atmospheric stability. The correlation coefficient for the results in Fig. 6 is approximately 0.75 and is greater than that of Kimura and Takahashi (1991). These results provide confidence in the model as experimental tools that can be used to examine the change of a local wind system, and a temperature distribution due to land-use alteration.

3.2 Change in the local wind system due to land-use alteration

In this section, estimates are given of the change in the local wind system due to land-use alteration during the 85 year period. The model simulated wind distribution (at z^* = 125 m) at 1500 LST for Case 1 (1985), Case 2 (1950), and Case 3 (1900) are shown in Figs. 7a, 7b, and 7c, respectively.

In Case 1, the southern part of the Kanto Plain is dominated by southerly winds, i.e., sea breezes from Tokyo Bay and Sagami Bay. These sea breezes form a wind convergence zone from Tokyo Bay toward the west of Urawa. On the other hand, the northern part of the Kanto Plain is covered by easterly and southeasterly winds. The easterly winds around

Table 7. Initial conditions for the model integration.

Initial surface potential temperature	25°C at the sea level
Initial vertical gradient of θ	0.0062°C m^{-1} (below 1000 m)
	0.0047°C m^{-1} (above 1000 m)
Initial surface relative humidity	82 %
Initial gradient of relative humidity	−0.0098 % m^{-1}
Initial wind speed	0 m s^{-1} (at all level)

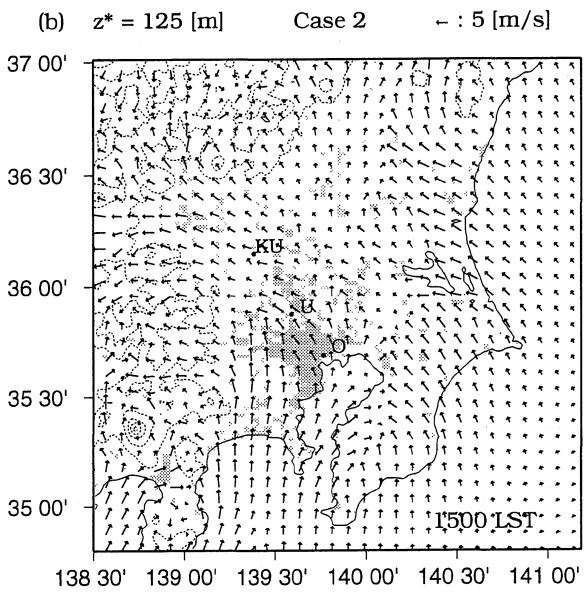

Fig. 7b. Same as Fig. 7a, but for Case 2.

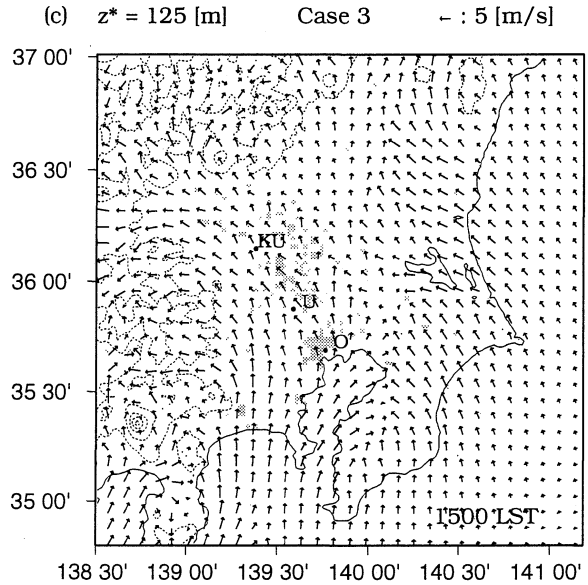

Fig. 7c. Same as Fig. 7a, but for Case 3.

Kounosu (see Fig. 2) flow toward the slope of the mountain located on the west of the Kanto Plain and the Tokyo metropolitan area. The northeasterly wind around Kounosu is thermally induced by the existence of the Tokyo metropolitan area located to the south of Kounosu. This will be discussed in detail in a later section. It should be also noted that there is a weak wind zone around Ageo located to the north of Urawa. These southerly and easterly winds produce strong convergence. This prominent convergence zone is located at the northern end of the Tokyo metropolitan area, and has been observed during field experiments by Yoshikado and Kondo (1989).

For Case 2 and Case 3, southerly and southeasterly wind penetrates further inland than that in Case 1, and dominate over the entire Kanto Plain. A strong convergence zone, a weak wind zone, and surface inflow toward the urban area are not found around the northern end of the Tokyo metropolitan area, Ageo, and Kounosu, respectively. In order to clarify the onset of the sea breeze, Fig. 8 shows the temporal variations of the horizontal wind (at $z^* =$ 125 m) during daytime hours along horizontal line from Shinkiba to Maebashi. The results for Case 1 and Case 3 are given in Figs. 8a and 8b, respectively. The shifts in the wind direction are mainly attributed to the sea breeze.

When examining Case 1, the sea breeze develops with time, and arrives at Otemachi around 1000 LST, and at Nerima around 1200 LST. The sea breeze front lingers off Nerima for three hours, reaching Urawa around 1500 LST. The sea breeze front, then, lingers off Urawa for two hours, reaching Ageo around 1700 LST. These features coincide with the observed results by Yoshikado and Kondo (1989). At the further inland sites, the speed of the local winds is enhanced during this time. These local winds are induced by the topography (Kondo 1990). Another important point is that the wind speed has been near calm until 1300, and 1500 LST around Urawa and Ageo, respectively. It should be also noted that there is a northerly wind around Urawa at 1400 LST.

For Case 3, the sea breeze develops with time, and arrives at Otemachi around 1000 LST. Afterward, the sea breeze continues to develop, arriving at Urawa around 1400 LST and at Ageo around 1500 LST. Consequently, the wind direction shifts from the east to southeast at inland stations. At

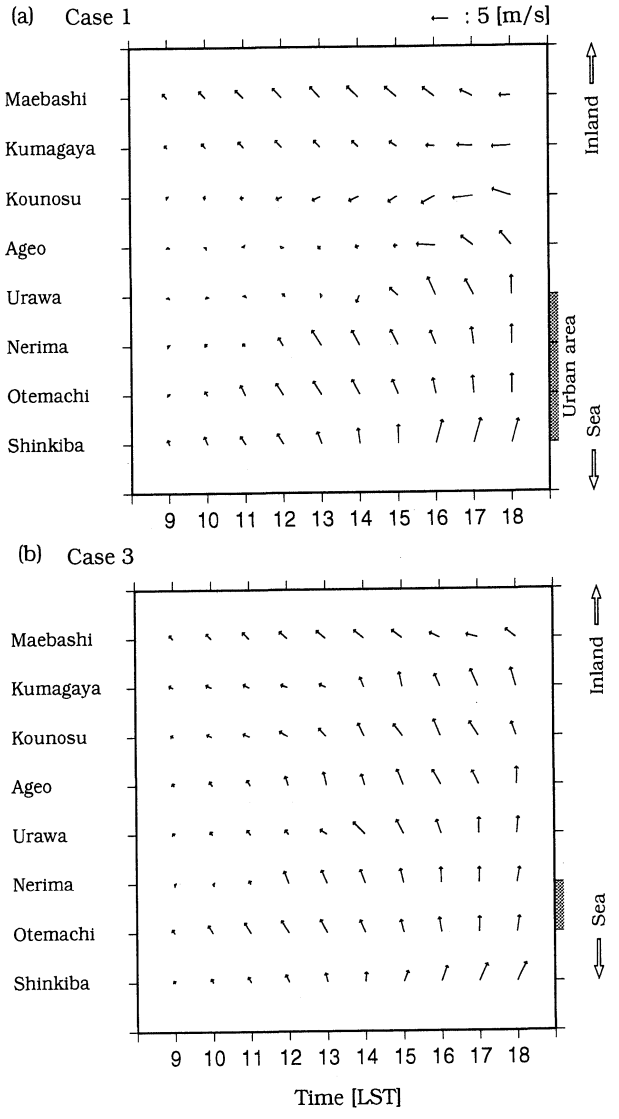

Fig. 8. Time variations of wind vectors in the horizontal plane along the points shown in Fig. 2, calculated for (a) Case 1 and (b) Case 3. The shaded areas indicate the urban area.

the further inland sites, the speed of the local winds is enhanced during this time. In addition, it seems that the wind speed of Case 3 is smaller than that of Case 1 over the southern part of the Kanto Plain. From the above results, it is found that the land-use alteration modifies the local wind system over the Kanto Plain. In particular, the simulated sea breeze front has become more clearly defined around the northern end of the Tokyo metropolitan area, and the north component of the wind velocity has become stronger around Ageo and Kounosu located north of Urawa. Moreover, the time required for sea breezes to reach inland areas has been delayed by two hours.

3.3 Temperature distribution change due to land-use alteration

The model simulated temperature (at $z^* = 10$ m) at 1500 LST for Case 1, Case 2, and Case 3 are given in Figs. 9a, 9b, and 9c, respectively.

With respect to Case 1, the region of temperatures higher than 31°C covers the entire Kanto Plain. The region over 32°C covers the entire northwestern area of the Kanto Plain, coastal areas of the Tokyo Bay, and expands northward along 139.7 E longitude. The region having temperatures higher than 33°C is distributed to the northwest of Tokyo. The region having temperatures higher than 34°C is not found in the central part of Tokyo, but is found rather around Urawa, located at the northern end of the Tokyo metropolitan area. It appears that the highest temperature region coincides with the convergence zone, and the weak wind zone is located north of it. These results suggest that urban areas around Urawa are 2–3°C warmer than their rural surrounding. Strong horizontal temperature gradients are found around the northern end of the Tokyo metropolitan area, the furthest inland area, and coastal area.

For Case 2, the region of temperatures higher than 31°C is similar to Case 1 but smaller than that in Case 1. The region over 32°C is smaller than that in Case 1 and not shown in the coastal area of the Tokyo Bay. The region having temperatures higher than 33°C is found in the west of Urawa, however not in the east of Urawa. The region having a temperature higher than 34°C is not found in the Kanto Plain. With Case 3, the region of temperatures higher than 31°C and 32°C are the smallest among the three cases. The region over 33°C is not found in the Tokyo metropolitan area. A temperature higher than 34°C is not found in the Kanto Plain.

Figure 10 indicates that the high temperature region expanded as urbanization advanced. The warming is found over the Tokyo metropolitan area, northwestern part of the Kanto Plain, and around some cities located at the northern part of the plain. The warming during the period is clearer along the boundary of the Tokyo metropolitan area than in the central part of Tokyo, and its average warm bias is 2–3°C. In particular, an area of the most prominant warming is found in the northern end of the urban area with the maximum value of 3–4°C. On the other hand, the urbanization that occurred over the last 35 years of the period account for an average warm bias of 1–2°C and the maximum value of 2–3°C from the comparison of Figs. 9a and 9b, although the figure of the difference is omitted.

Vertical profiles of potential temperature above Urawa for Case 1 and Case 3 are shown in Figs. 11a and 11b, respectively.

After sunrise, a convective mixed layer develops in both cases. The growth and heating rate of the

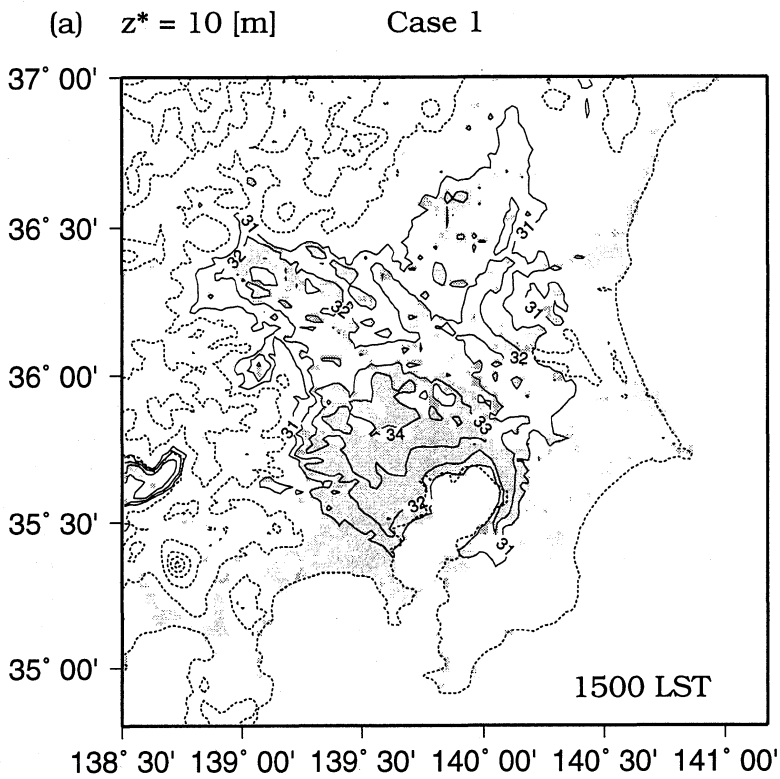

Fig. 9a. Temperatures at the $z^* = 10$ m level for 1500 LST, calculated for Case 1 . The contour interval is 1°C. The shaded areas indicate the urban area. The broken lines indicate topography contour line, and the contour interval is 600 m.

mixed layer in Case 1 are greater than those in Case 3. Therefore, the depth of the mixed layer in Case 1 are about 100, 400, and 1000 m higher than those in Case 3 respectively at 0900, 1200, and 1500 LST. The mean mixed layer potential temperature in Case 1 are about 1, 1.5, and 2.5°C higher than that in Case 3 respectively at 0900, 1200, 1500 LST. It is considered that these differences are mainly due to the change of heating associated with land-use alteration, from grassland and paddy field to urban (see Fig. 3). Namely, they are caused by the increase of the sensible heat flux associated with the change of the Bowen ratio, as mentioned in a later paragraph. The height of the mixed layer in Case 1, at 1500 LST, has approximately jumped to 2000 m. This result supports the results in Section 3.2, the arrival of the sea breeze front with strong convergence and upward flow in the lower mixed layer.

In order to estimate the change in the heating process with land-use alteration, heat balance in an atmospheric column is analyzed. The time integrated sensible heat flux from ground surface (Q_H), the cumulative heat in an atmospheric column (Q_C), and the cumulative horizontal heat flux divergence (Q_{DIV}) are difined as Eqs. (12)–(14).

$$Q_H = \int_{t_0}^{t_1} H dt, \tag{12}$$

$$Q_C = \frac{1}{(t_1 - t_0)} \int_{z_G}^{z_r} c_p \rho_0 (\theta_1 - \theta_0) dz, \tag{13}$$

and

$$Q_{DIV} = Q_H - Q_C. \tag{14}$$

Here, H is the sensible heat flux from the surface, t_0 is the base time (0600 LST) of the analysis, and t_1 the object time. In addition, θ_0 is the potential temperature at the base time t_0, and θ_1 is the potential temperature at the object time t_1. For example, Q_C at 1500 LST equals the difference between the profiles at 0600 LST and 1500 LST in Fig. 11. The cumulative heat Q_C is nearly proportional to the negative anomaly of the surface pressure from the base time. The cumulative horizontal heat flux divergence Q_{DIV} is estimated as the residual.

The results for Case 1 and Case 3 are given in Figs. 12a and 12b, respectively.

With regard to Case 1, Q_H (open circle) exhibits a large growth rate of 0–9.4 M J m^{-2} during the daytime. This is mainly because the Bowen ratio is very large over this area. The cumulative heat Q_C (solid circle) increases along with Q_H from 0600

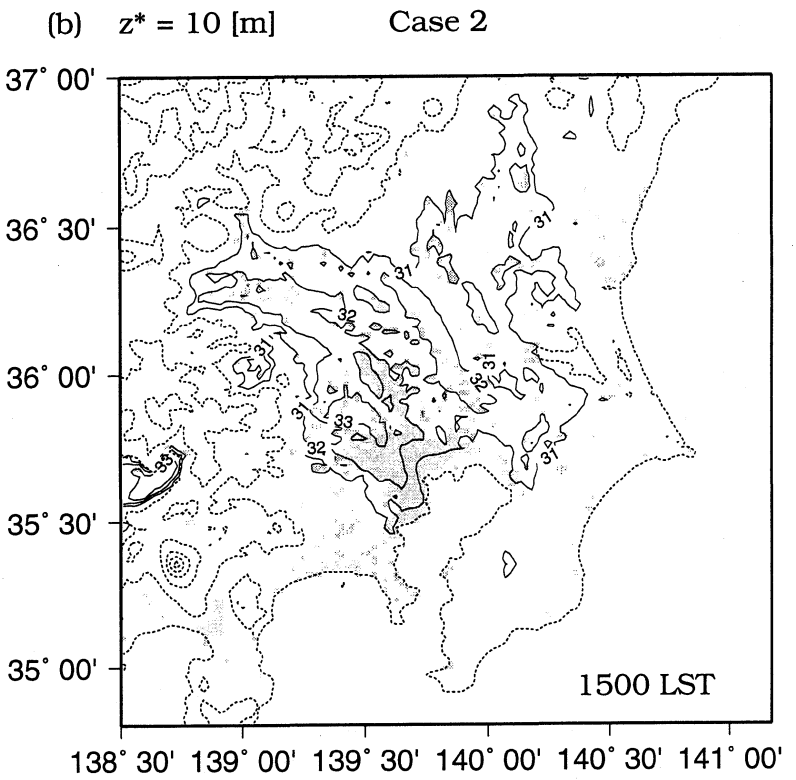

Fig. 9b. Same as Fig. 9a, but for Case 2.

LST to 1400 LST, because the weak winds have covered over the area during the time as mentioned in Section 3.2. It is considered that a relatively low pressure zone has been formed over the area during this time. At 1500 LST, the increasing rate of Q_C becomes smaller rapidly due to the increase of Q_{DIV} (open square), which represents the arrival of the sea breeze front, as mentioned in Section 3.2. Here, what we want to emphasize is that the change of Q_{DIV} is attributed to the sum of an advection by the sea breeze inflow itself and the cooling by the divergence flow near the top of the mixed layer associated with upward flow. After 1500 LST, Q_C continues to decrease and the advance of the sea breeze front accelerates due to the enhanced surface pressure (Yoshikado and Kondo 1989). These changes indicate that the delay of the arrival of the sea breeze front played significant roles in the formation of the daytime heat island around Urawa. Consequently, the maximum value of Q_C appears at 1500 LST, having a magnitude of about 7.4 M J m^{-2}.

For Case 3, Q_H exhibits a smaller growth rate of 0–5 M J m^{-2} than that of Case 1, due to land-use difference. The cumulative heat Q_C approximately fluctuates along with Q_H because fluctuation of Q_{DIV} is small during the daytime.

From the above results, it is found that the maximum magnitude of Q_C, in particular, during the daytime, increases with urbanization. It is considered that the sea breeze front shown in Fig. 7a is formed, through the thermally induced pressure gradient. Contrary to this, this sea breeze front modified by the land-use alteration also strongly affects the daytime heat island in 1985. These imply that interaction of the boundary layer heating and the sea breeze front has a strong effect on creating the daytime heat island in 1985. Consequently, we can conclude that the warming around Urawa results from the enhanced sensible heat flux and the change of the interaction associated with it.

4. Remarks and conclusions

The temporal change of daytime heat island and sea breeze associated with the development of an urban area has been estimated by using realistic past land-use data. The domain of interest was the Kanto Plain, including the Tokyo metropolitan area, which had rapidly developed into one of the largest urban areas in the world during a period of 85 years. Three time periods were investigated, the time around the years 1985, 1950, and 1900. The summary of the results can be split into three components, with focus on the local climate change during the 85 year period:

(1) Simulation of undisturbed summer day for 1985

The simulated surface temperature distribution and wind system in 1985 agreed with those observed

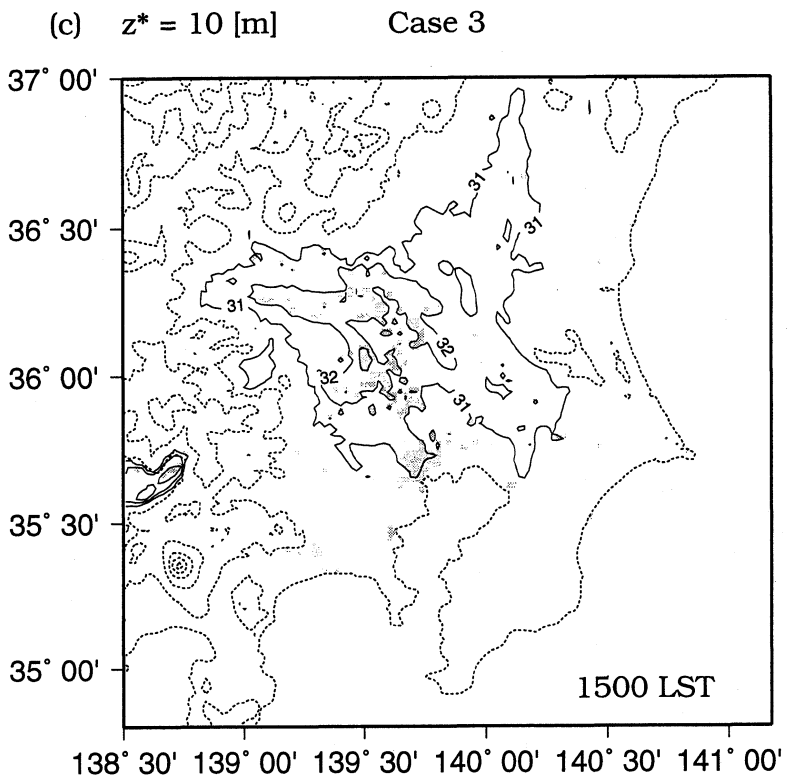

Fig. 9c. Same as Fig. 9b, but for Case 3.

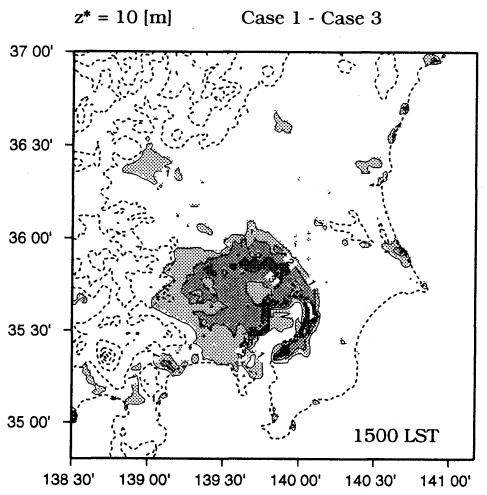

Fig. 10. The difference in the simulated temperature between Case 1 and Case 3 (Case 1 – Case 3). Values greater than 3°C are indicated by the heavy shading, values greater than 2°C are indicated by the medium shading, and values greater than 1°C are indicated by the light shading. The broken lines indicate topography contour line, and the contour interval is 600 m.

under the summer synoptic condition characterized by weak gradient wind and almost clear sky. In particular, the correlation coefficient between the simulated and observed temperatures was about 0.75.

(2) Change of the sea breeze

The land-use alteration modified the local wind system over the northern part of the Kanto Plain, as well as over the southern part of the Kanto Plain, including the Tokyo metropolitan area. The simulated sea breeze front became more clearly defined around the northern end of the Tokyo metropolitan area. The time required for sea breezes to reach inland areas increased by two hours.

(3) Change in the daytime heat island

The urbanization on the Tokyo metropolitan area during the 85 year period accounted for an average warm bias of 2–3°C, while that during the last 35 years of the period accounted for an average warm bias of 1–2°C. The warming is clearer along the boundary of this urban area than in the central part of Tokyo. In particular, the region of the most prominent warming is found in the northern end of the Tokyo metropolitan area and the maximum value is 3–4°C and 2–3°C during the 85 year period, and the last 35 years of the period, respectively. The above warming results from the enhanced sensible heat flux and the change of interaction between the boundary layer heating and the sea breeze front.

Kimura and Takahashi (1991) reported that the temperature above Tokyo is quite high and formed a daytime heat island. In the present paper, the high

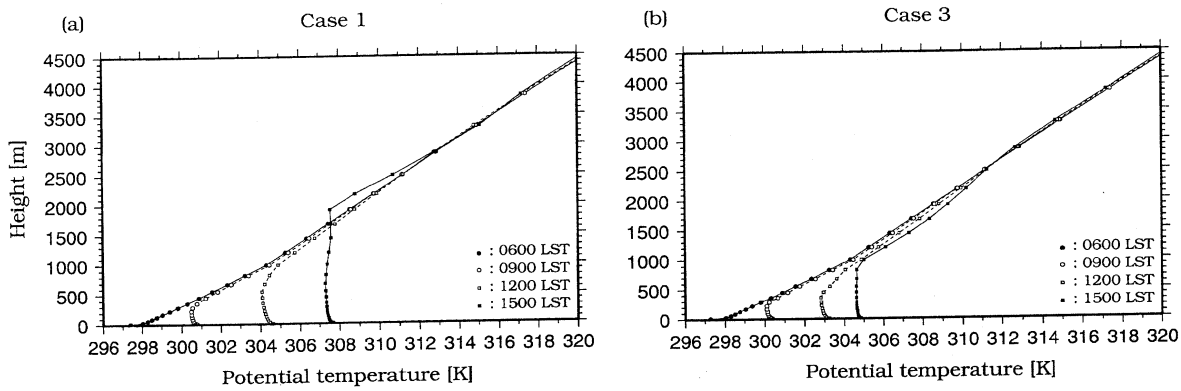

Fig. 11. Vertical profiles of potential temperature at Urawa for (a) Case 1, and (b) Case 3. The solid line with solid circles represent 0600 LST, dotted line with open circles 0900 LST, dotted line with open squares 1200 LST, and the solid line with solid squares 1500 LST.

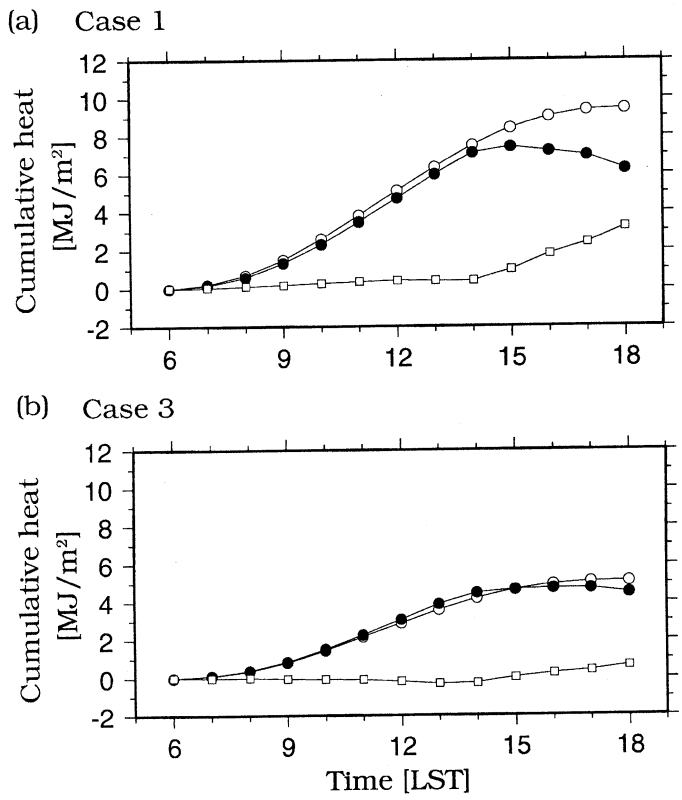

Fig. 12. Time series of cumulative heat around Urawa for (a) Case 1, and (b) Case 3. The open circles denote the time integrated heat flux from ground surface, Q_H. The solid circles represent the cumulative heat in atmospheric column, Q_C. The open squares represent the cumulative heat of the vertically integrated horizontal heat flux divergence, Q_{DIV}. These terms are averaged values over the square region of 20 km (E–W) by 10 km (N–S) around Urawa.

temperature zone is confirmed to be distributed to the northwest of Tokyo as well as in the central part of Tokyo. It is believed that simulated results help to know the real condition of the daytime heat island over the Kanto Plain. Through the simulation and heat budget analysis, it was found that the delay of the arrival of the sea breeze front plays important roles in the formation of the daytime heat island around Urawa.

Yoshikado and Kondo (1989) and Yoshikado (1990) found that the convergence zone is formed by the sea breezes from Sagami Bay and Tokyo Bay and this sea breeze front tended to remain around Urawa located northwest of Tokyo by the analysis of data observed during the field experiments.

Moreover, Yoshikado (1992, 1994) simulated the interaction between the land-sea breeze and the urban heat island circulation, using a two-dimensional

model which roughly corresponded to the conditions around Tokyo. In his study, the sea surface temperature is a constant value, land surface temperature experiences a diurnal variation, and the urban surface is assumed to be warmer than the rural surface. It was pointed out that the sea breeze front tended to remain over the city as a result of the urban heat island effect. This tendency was basically controlled by the characteristics of urban area: the size, distance from the sea, and intensity of the urban heat island. The present results with the realistic terrain and land-use data coincided with the features observed by Yoshikado and Kondo (1989) and Yoshikado (1990), and the features simulated by Yoshikado (1992, 1994).

According to the observed data, the daily maximum temperature over the Tokyo metropolitan area has increased by about 1°C during a 30 year period (Fig. 1). This increase nearly equals to that calculated in the present study. Figure 1 also shows a temperature increase of 1–1.5°C over 30 years in the area around Urawa and a decrease along the coastal area of the Kanto Plain. This temperature increase is less than calculated in the present study. On the other hand, the temperature increase in Fig. 1 over the furthest inland area is more than that in the present study. It should be noted that the analysis of the former observed increase did not consist of only undisturbed summer days, but also the other days. That is, the result shown in Fig. 1 includes westerly gradient wind days on which the daily maximum temperature over the inland area tended to be high (Fujibe 1998), the other strong gradient wind days, and rainy days on which daytime heat island is not clearly seen. In addition, the observed warming probably includes a component of the global climate change, and the observation term (1946–1976) differed from the simulation term (1900, 1950, 1985) in this study. Considering the differences of the above mentioned synoptic conditions and the object term, the tendency of the distribution of the warming area roughly agreed with the results calculated in the present study. The results of Fujibe (1994) also roughly agreed with the present results. Such an agreement means that the results of the numerical simuations in the present study support these findings obtained from the observation.

Anthropogenic heat was not considered in the present model, in order to focus on the effects of land-use alteration. The effects of cloud cover and gradient wind were also not considered in the model. Local climate change due to anthropogenic heat and cloud cover are important, judging from the two main climate elements, that is, energy and water. In fact, it is well known that the effects of the anthropogenic heat on the heat island is larger during nighttime than daytime (i.e., Kimura and Takahashi 1991; Ichinose 1999). In addition to the general feature of the heat island, Ichinose (1999) describes a fine structure of a heat island in Tokyo using much detailed maps of anthropogenic heat and land-use, and points out that a internal heat island may exist at several busy quarters cities in Tokyo. Estimates of the local climatic change over the Tokyo metropolitan area due to anthropogenic heat, cloud cover, and gradient wind will be the subject of a future study.

Acknowledgments

The authors are grateful to Prof. Himiyama of the Hokkaido Kyouiku University for providing the land-use data and to Dr. Fujibe of the Meteorological Research Institute for providing the figure of daily maximum temperature change. The authors also wish to thank Dr. Yamazawa of Japan Atomic Energy Research Institute for his comments on the surface parameters. Free software 'GMT' (the Generic Mapping Tools) was used in drawing the figures.

Appendix

List of Symbols

c_p specific heat of air,

f Coriolis parameter,

g acceleration of gravity,

H sensible heat flux,

K_H horizontal exchange coefficient,

K_m vertical exchange coefficient of momentum,

K_h vertical exchange coefficient of heat,

lE latent heat flux,

p pressure,

p_{00} reference pressure,

q specific humidity,

q_* friction specific humidity,

R_d gas constant for air,

t time,

u east-west component of wind velocity,

u_* friction velocity,

v north-south component of wind velocity,

w vertical component of wind velocity,

z_G ground elevation,

z_T height of the model atmosphere top,

z^* vertical coordinate (terrain following),

θ potential temperature,

θ' $= \theta - \Theta$,

θ_* friction potential temperature,

Θ mean potential temperature,

π Exner's function,

π' $= \pi - \Pi$,

Π mean Exner's function,

ρ_0 mean fluid density,

τ momentum flux.

References

Anthes, R.A., E-Y. Hsie and Y.-H. Kuo, 1987: Description of the Penn State / NCAR Mesoscale Model Version 4 (MM4). *NCAR Technical Note*, NCAR / TN-282+STR, 66pp.

Bhumralkar, C.M., 1975: Numerical experiments on the computation of ground surface temperature in an atmospheric general circulation model. *J. Appl. Meteor.*, **14**, 1246–1258.

Bornstein, R.D., 1986: Urban climate models: nature, limitations and applications. WMO, **652**, 237–276.

Deardorff, J.W., 1978: Efficient prediction of ground surface temperature and moisture, with inclusion of a layer of vegetation. *J. Geophy. Res.*, **83**, 1889–1903.

Fujibe, F., 1994: Long-term falling trends of pressure over the Kanto Plain as evidence of increasing heat content in the lower atmosphere in the daytime of the warm season. *J. Meteor. Soc. Japan*, **72**, 785–792.

———, 1998: An increasing trend of extremely hot days in the inland of the Kanto Plain and its relation to urban effects. *Tenki*, **45**, 643–653 (in Japanese).

——— and T. Asai, 1979: A study of local winds in Kanto distric. Part 1: Structures of wind systems with diurnal variation. *Tenki*, **26**, 595–604 (in Japanese).

——— and T. Asai, 1980: Some features of a surface wind system associated with the Tokyo heat island. *J. Meteor. Soc. Japan*, **58**, 149–152.

Gamo, M., 1985: Seasonal change of the mixed layer structure at Tsukuba. *J. Meteor. Soc. Japan*, **63**, 60–74.

Garratt, J. R., 1978: Transfer characteristics for a heterogeneous surface of large aerodynamic roughness. *Quart. J. Roy. Metor. Soc.*, **104**, 491–502.

Hjelmfelt, M.R., 1982: Numerical simulation of the effects of St. Louis on mesoscale boundary-layer airflow and vertical air motion: Simulations of urban vs non-urban effects. *J. Appl. Meteor.*, **21**, 1239–1257.

Himiyama, Y., 1998: Land use/cover changes in Japan: from the past to the future, *Hydrol. Process.*, **12**, 1995–2001.

Ichinose, T., K. Shimodozono and K. Hanaki, 1999: Impact of anthropogenic heat on urban climate in Tokyo, *Atmos. Environ.*, **33**, 3897–3909.

Kimura, F. and S. Arakawa, 1983: A numerical experiment of the nocturnal low level jet over Kanto plain. *J. Meteor. Soc. Japan*, **61**, 848–861.

——— and S. Takahashi, 1991: The effects of land-use and anthropogenic heating on the surface temperature in the Tokyo metropolitan area: A numerical experiment. *Atmos. Environ.*, **25B**, 155–164.

Klemp, J.B. and D.R. Durran, 1983: An upper boundary condition permitting internal gravity wave radiation in numerical mesoscale models. *Mon. Wea. Rev.*, **111**, 430–444.

Kondo, H., 1990: A numerical experiment of the interraction between sea breeze and valley wind to generate the so-called "extended sea breeze". *J. Meteor. Soc. Japan*, **68**, 435–446.

——— and H. Yoshikado, 1988: The characteristic of surface wind in Japan analyzed by AMeDAS DATA (part 2), -Monsoon and land-sea breezes-. *Bulletin of the national research institute for pollution and resources*, **17**, 29–40 (in Japanese).

Kondo, J. and H. Yamazawa, 1986: Aerodynamic roughness over an inhomogeneous ground surface. *Bound. - Layer Meteor.*, **35**, 331–348.

———, T. Nakamura, and T. Yamazaki, 1991: Estimation of the solar and downward atmospheric radiation. *Tenki*, **38**, 41–48 (in Japanese).

——— and T. Watanabe, 1992: Studies on the bulk transfer coefficients over a vegetated surface with a multilayer energy budget model. *J. Atmos. Sci.*, **49**, 2183–2199.

Mellor, G.L. and T. Yamada, 1974: A hierarchy of turbulence closure models of planetary boundary layers. *J. Atmos. Sci.*, **31**, 1791–1806.

Nakagawa, K. and Y. Ooi, 1992: The surface albedo distribution and its seasonal change over the Nagaoka area, Niigata prefecture, Central Japan, estimated with LANDSAT/MSS data. *Geographical Review of Japan*, **65A-10**, 769–790 (in Japanese).

Ogura, Y. and N.A. Phillips, 1962: Scale analysis of deep and shallow convection in the atmosphere. *J. Atmos. Sci.*, **19**, 173–179.

Orlanski, I., 1976: A simple boundary condition for unbounded hyperbolic flows. *J. Comp. Phys.*, **21**, 251–269.

Seaman, N.L., F.L. Ludwig, E.G. Donall, T.T. Warner and C.M. Bhumralker, 1989: Numerical studies of urban planetary boundary-layer structure under realistic synoptic condition. *J. Appl. Meteor.*, **28**, 760–781.

Taha, H., St. Konopacki and S. Gabersek, 1999: Impacts of large-scale surface modifications on meteorological conditions and energy use: A 10-region modeling study., *Theor. Appl. Climatol.*, **62**, 175–185.

Wessel, P. and W.H.F. Smith, 1995: New version of the Generic Mapping Tools released., *EOS Trans. Amer.*

Geophys. U., **76**, 329 pp.
Yamamoto, G., 1952: On a radiation chart. Sci. Rep. Tohoku Univ., Ser. 5., *Geophys.*, **4**, 9–23.
Yoshikado, H., 1990: Vertical structure of the sea breeze penetrating through a large urban complex. *J. Appl. Meteor.*, **29**, 878–891.
———, 1992: Numerical study of the daytime urban effect and its interaction with the sea breeze. *J. Appl. Meteor.*, **31**, 1146–1164.
———, 1994: Interaction of the sea breeze with urban heat islands of different size and locations. *J. Meteor. Soc. Japan*, **72**, 139–143.
——— and H. Kondo, 1989: Inland penetration of the sea breeze over the suburban area of Tokyo. *Bound.-Layer Meteor.*, **48**, 389–407.

土地利用形態の変遷が首都圏の海風と日中のヒートアイランドに及ぼす影響

日下博幸
（電力中央研究所環境科学部）
木村富士男
（筑波大学地球科学系）
平口博丸・水鳥雅文
（電力中央研究所環境科学部）

過去85年間（1900–1985）の土地利用変化が海風と日中のヒートアイランドの変化に及ぼす影響について数値モデルを用いて検討した。解析対象領域は首都圏を含む関東平野（150000 km^2）である。首都圏はこの平野の南側に位置しており、東京とその近郊に広がる数多くの都市から形成されている。首都圏の水平規模は半径約40 kmであり、過去85年間で約4倍に広がっている。解析対象日は一般風の弱い夏季晴天日であり、用いた数値モデルは静力学平衡を仮定した非弾性近似方程式系の三次元モデルである。1985年の土地利用データを用いたシミュレーション結果と観測値がおおむね一致していることを確認した後、1950年および1900年の土地利用データを用いたシミュレーションを行った。以下に主な二つの結果を記す。(1) 土地利用変化に伴い、関東平野の風系は変化する。海風前線は首都圏の北側境界付近で強まり、平野の内陸部への進入時刻は1～2時間遅れる。(2) 土地利用変化に伴う日最高気温の上昇傾向は首都圏と関東平野の北西部で見られる。とりわけ、このような昇温傾向は首都圏の北側境界付近において顕著であり、この地域では3～4°C/85年、2～3°C/35年の上昇が認められる。上記の昇温は顕熱フラックスの増加および、大気境界層の加熱と海風前線の相互作用の変化によって生じていると考えられる。